Earthquakes and Structures, *Vol. 7, No. 5 (2014) 609-626*
DOI: http://dx.doi.org/10.12989/eas.2014.7.5.609

Advancing behavioral understanding and damage evaluation of concrete members using high-resolution digital image correlation data

Drit Sokoli[1a], William Shekarchi[1b], Eliud Buenrostro[2c] and Wassim M. Ghannoum*[2]

[1]Department of Civil Architectural and Environmental Engineering, University of Texas at Austin 301 E. Dean Keeton St. STOP C1700, Austin, TX, USA
[2]JQ Dallas, 2015 Commerce St., Dallas, TX, USA

(Received April 20, 2014, Revised May 6, 2014, Accepted May 7, 2014)

Abstract. The capabilities of a high-resolution Digital Image Correlation (DIC) system are presented within the context of deformation measurements of full-scale concrete columns tested under reversed cyclic loading. The system was developed to have very high-resolution such that material strains on the order of the cracking stain of concrete could be measured on the surface of full-scale structural members. The high-resolution DIC system allows the measurement of a wide range of deformations and strains that could only be inferred or assumed previously. The DIC system is able to resolve the full profiles of member curvatures, rotations, plasticity spread, shear deformations, and bar-slip induced rotations. The system allows for automatic and objective measurement of crack widths and other damage indices that are indicative of cumulated damage and required repair time and cost. DIC damage measures contrast prevailing proxy damage indices based on member force-deformation data and subjective damage measures obtained using visual inspection. Data derived from high-resolution DIC systems is shown to be of great use in advancing the state of behavioral knowledge, calibrating behavioral and analytical models, and improving simulation accuracy.

Keywords: digital image correlation; deformations; strains, damage index; concrete

1. Introduction

Traditionally, the structural engineering field has been concerned with limiting structural forces through strength-based design, and limiting cracking in concrete members at service-load levels. However, in the inelastic range of behavior, force becomes a poor measure of damage and performance, and limiting deformations is the limit-state of choice. This is particularly the case when structures are subjected to relatively large inelastic deformations during extreme loading

*Corresponding author, Wassim M. Ghannoum, PhD, E-mail: ghannoum@mail.utexas.edu
[a]Master Student, E-mail: drit@utexas.edu
[b]Ph.D. Student, E-mail: wshekarchi@utexas.edu
[c]Project Engineer, E-mail: ebuenrostro@jqeng.com

http://www.techno-press.org/?journal=eas&subpage=7 ISSN: 2092-7614 (Print), 2092-7622 (Online)

events, such as earthquakes. In such cases, the structural engineering community is gradually moving towards performance-based design and evaluation procedures that incorporate strength, deformation, and damage limit-states (e.g., FEMA 273, ASCE 41-06). Based on a structure's occupancy and its need to retain functionality after a major seismic event, various performance objectives may be targeted at various hazard levels. Performance objectives can range from Immediate Occupancy to Collapse Prevention (ASCE 41-06), and ideally should have intermediate objectives that target limited structural damage and repair time. Key to moving towards deformation- and damage-based design methodologies is the ability to simulate structural behavior and estimate damage progression from low deformation levels to complete loss of strength.

Experimental testing of structural members provides the structural engineering field with benchmark data to calibrate strength, stiffness, and damage models. Comprehensive measurement of deformations and damage during structural testing is necessary to fully understand and quantify member deformations, stiffness, and damage progression. Yet traditional instrumentation and measurement techniques suffer several limitations that have hindered progress. Traditional instrumentation that monitors member deformations consists of linear voltage displacement transducers (LVDTs), wire pots, and strain gages. Such instrumentation can only provide deformation data at limited locations and suffers from loss of measuring capabilities as damage progresses. Moreover, traditional damage measurement techniques are typically obtained using proxy force-deformation relations or subjectively through manual crack-width measurements and visual inspections of damage.

Recent advances in Digital Image Correlation (DIC) systems have allowed for the comprehensive distributed measurement of surface deformations that could not be achieved previously. DIC systems use digital cameras to track changes between consecutively recorded images to output two- or three-dimensional deformation measurements. If a DIC system can resolve movements on the order of a $1/100^{th}$ of an inch (0.25 mm), the distribution of deformations can be tracked over the entire area of a structural member. If a DIC system can resolve movements on the order of $1/5000^{th}$ of an inch (0.005 mm), material surface strains can be measured reliably for full-scale structural members. A high-resolution DIC system was recently developed at the University of Texas at Austin (UT). The UT Vision System (UTVS) is able to resolve surface strains on the order of 10^{-4} over a field of view of 96" (2440 mm) and gage length of 2.5 in. (63 mm). The UTVS can record surface deformation and strains to such a fine resolution that numerous quantities that could only be inferred previously can now be measured. The benefits of measuring distributed deformations and material strains for full-scale test specimens are discussed within the context of two experiments conducted on reinforced concrete columns. The potential for using high-resolution DIC data for damage quantification is also discussed. Particular emphasis is placed on the implications of the novel data on models estimating strength and stiffness measures that are critical for the seismic response of structures.

2. DIC versus traditional Instrumentation

Behavioral and analytical models are developed and calibrated based on measurements of member forces and deformations during structural testing. The total deformation of a structural member (Δ_T) can be broken down into three components: flexural (Δ_{FL}), shear (Δ_{SH}), and bar-slip (Δ_{BS}) deformations (Fig. 1). Based on current knowledge, shear deformations in concrete columns typically comprise about 5% of the total deformations, but can be more significant in shorter columns (Sezen and Moehle 2006). Flexural deformations typically comprise 40 to 60% of the total, while bar-slip induced deformations can comprise up to 40% of the total (Ghannoum and Moehle 2012a and b).

In the majority of structural tests, only the total lateral displacement is measured (Δ_T in Fig. 1). Therefore, in most cases many assumptions need to be made to deconstruct total deformations into the various deformation components. Consequently, deformation and stiffness models derived from global deformation data exhibit relatively large errors. In some limited tests, a coarse grid of LVDTs is applied to a frame member as illustrated in Fig. 2 (e.g., Saatcioglu and Ozcebe 1989; Lynn 2002; Sezen and Moehle 2006). Such grids allow for the deconstruction of member deformations into the various components at limited locations along member length. LVDT-based measurement systems, however, are limited in the number of measurement points due to instrument congestion issues. They are also sensitive to member damage that displaces the connection points of the instruments. Since LVDT systems rely on cumulative triangulation using several instruments, the loss of one instrument often results in the cascading loss of measurements of many points.

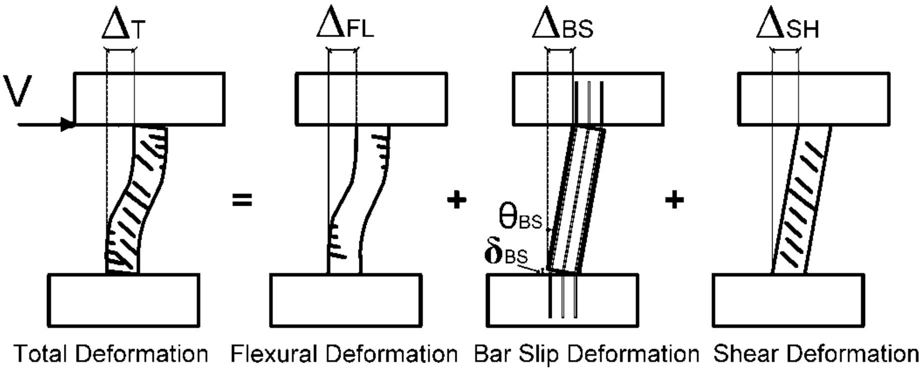

Fig. 1 Concrete column deformation components

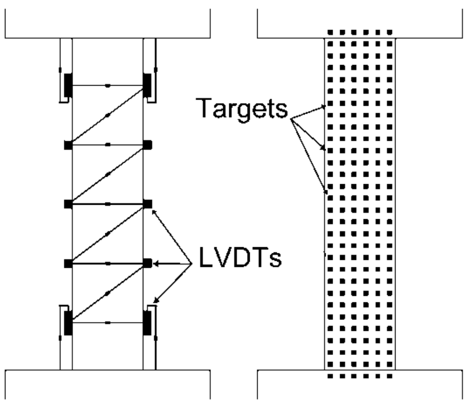

Fig. 2 LVDT vs. DIC measurement density

DIC measurement systems are able to track the movement of a dense grid of targets covering the entire surface of a member (Fig. 2). DIC measurements are damage-tolerant as the movement of each target is monitored independently such that the loss of one target due to member damage does not affect readings of other targets. DIC systems offer the structural engineering community new data from which member deformations can be deconstructed over a member's length, interactions between the various deformations can be observed, and new behavioral mechanisms can be uncovered. The distributed nature of DIC deformation data also allows the calibration of analytical models along the entire member as opposed to at member ends, as it is typically done using traditional LVDTs measurements.

As damage progresses during cyclic loading, it is useful to monitor and quantify the damage to identify demand parameters that cause various threshold damage levels. Traditionally, damage indices have been used to quantify member damage accumulation during structural testing. Most indices have been based on member lateral-force versus lateral-deformation relations because that data constituted the only objective measure extracted from traditional instrumentation. In some cases, the degree of damage in structural members was pegged to the relative magnitude of ductility demands and ductility capacities (IAAE 1996), while some damage indices have used concepts of dissipated energy, ductility, and degradation of stiffness to assess damage accumulation (e.g., Park 1985; Cosenza 1993). However, indices using global force-deformation relations are merely utilizing proxies to assess damage occurring along the length of a member, and may not correlate well with visible and repairable damage. Other types of damage measures include the area of concrete spalling and the width and extent of concrete cracking (e.g., Eleftheriadou 1999). However, given the manual and visual nature of those types of damage measurements, subjectivity and non-repeatability hinder comparative studies using results from different members and research teams.

DIC data can identify areas of deformation concentrations and quantify deformation increases in damaged regions. High-resolution DIC systems can track surface strains that allow for automated measurements of damage parameters such as crack widths and areas of concrete crushing. DIC systems can track all surface cracks and damage through material-strain thresholds, and provide objective and repeatable damage measures. DIC damage data can therefore be used reliably in comparative damage studies using test data from various structural testing programs.

3. Experiments

A high-resolution DIC system dubbed the UTVS was recently developed to deliver high-resolution surface strain measurements for full-scale structural members. The system consists of two 16MegaPixel cameras with low-noise CCD sensors (35 mm sensor format). A software package utilizing the Matlab Image Processing Toolbox (Mathworks 2014) and the NI Vision Development Module (National Instruments 2014) was developed to track the location of user-selected sub-images (i.e., targets). The system tracks target locations in each recorded frame using a Digital Image Correlation (DIC) algorithm. A calibration procedure adjusts for lens distortion and provides the necessary extrinsic and intrinsic camera parameters for the three-dimensional triangulation of target locations. The UTVS tracks surface movements to a resolution on the order of $1/25^{th}$ of a pixel for raw location data, and a $1/100^{th}$ of a pixel after smoothing is applied to the location data. For example, for a field of view of 96” × 64” (2440 × 1626 mm), raw location resolution would be 96" / 4872 pixels / 25 = 8×10^{-4} in. (0.02 mm) and smoothed resolution 2×10^{-4} in. (0.005 mm). The system is therefore able to resolve surface strains on the order of 10^{-4} over a field of view of 96" (2440 mm) and gage length of 2.5 in. (63 mm). The UTVS can record images at up to three frames per second but usually runs at a frame rate of 0.75 Hz. The UTVS software can calculate target movement from previously stored images and can therefore work with high-speed cameras to measure deformations during shaking table tests or tests under rapid loading rates (e.g., Ghannoum *et al*. 2012).

Results from two experiments conducted by the authors on reinforced concrete columns are presented to illustrate the potential benefits of using high-resolution DIC systems, such as UTVS, in structural testing. Experiment 1 was conducted on a column with a cross-section of 16x16in. (405 × 405 mm) and a clear height of 116 in. (2.95 m). The column had a shear span-to-depth ratio of 4.3. Longitudinal reinforcement consisted of 8 #8 (25 mm) longitudinal bars, which corresponded to a 2% longitudinal reinforcement ratio. The column was not seismically detailed. Transverse reinforcement consisted of #3 (10 mm) ties with 90° hooks spaced at 6 in. on center (152 mm). All steel reinforcement was ASTM A615 Grade 60 (420 MPa). The 28-day concrete compressive strength of the column was 3.3 ksi (23 MPa). The column was tested under symmetric double curvature with zero rotation maintained at top and bottom. Quasi-static cyclic lateral loading was applied to the column with increasing amplitudes. The loading protocol consisted of three lateral displacement cycles at each displacement increment. Throughout the test, a constant compressive axial load of 350 kips (1557 kN) was applied to the column, which corresponded to $0.41A_gf'_c$; where A_g = gross sectional area and f'_c = concrete compressive strength. The column exhibited relatively low ductility capacity, initiated loss of lateral strength, and subsequently sustained axial failure at 3.0% drift ratio (= lateral drift / column clear height).

Experiment 2 was conducted on a reinforced concrete column with cross-section dimensions of 18×18 in. (457×457 mm) and a clear height of 84 in. (2.1 m) (Fig. 4). The column has a shear span-to-depth ratio of 2.7. It had 12 #10 (32 mm) longitudinal bars corresponding to a longitudinal reinforcement ratio of 4.7%. The transverse reinforcement consisted of #5 (13 mm) hoops with 135° hooks spaced at 5.5 in. (14 cm) on center (Fig. 4). All steel reinforcement was Grade 60 ASTM A706. The concrete compressive strength at testing was 4.2 ksi (29 MPa). The column was tested in symmetric double curvature with zero rotation maintained at both ends. The loading protocol consisted of two lateral displacement cycles at each displacement increment as per FEMA 461 recommendations. A constant compressive axial load of 370 kips (1646 kN) was maintained during the test. This load corresponded to $0.27A_gf'_c$. The column


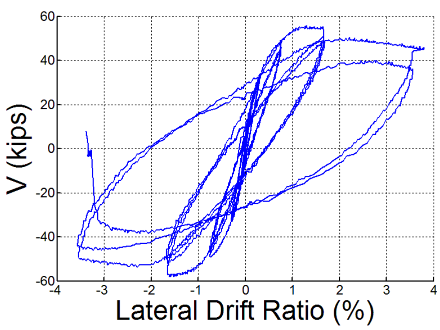

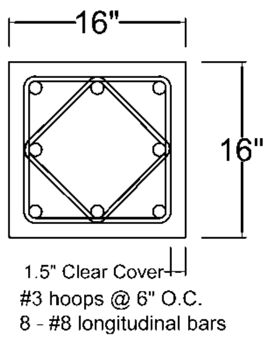

Fig. 3 Experiment 1(1 in. = 25.4 mm, 1 kip = 4.45 kN)

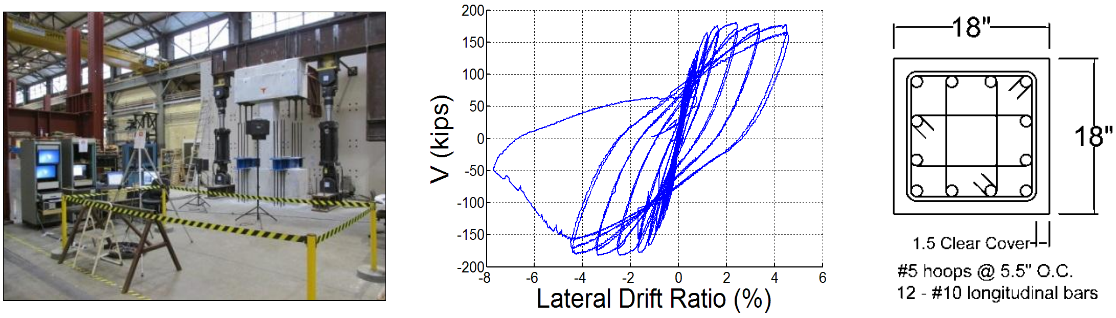

Fig. 4 Experiment 2 (1 in. = 25.4 mm, 1 kip = 4.45 kN)

showed relatively high ductility, reaching a drift ratio of 6% before initiating lateral and axial strength loss almost concurrently. The test was continued under reduced axial load and finally stopped at a drift ratio of 9.5% when the axial capacity dropped to less than 200 kips (890 kN) and the lateral strength dropped below 25%.

In both experiments, the UTVS was used to measure deformations and extract damage indices. In the first experiment, targets were spaced at 3 in. (76 mm) on center, with 6 targets fitting per horizontal row. In the second experiment, targets were spaced at 2.75 in. (70 mm) on center, with 7 targets fitting per horizontal row. An additional row of targets was placed in each footing to allow for measurement of deformations at the column-to-footing interface (i.e., bar-slip induced deformations).

4. Member deformations

Deformations of reinforced concrete structural members subjected to lateral loads can be divided into flexural, shear, and bar-slip deformations (Fig. 1). Each of these deformation components exhibits a linear force-deformation relation at low demands and inelastic behavior at larger demands. Deformation components can be coupled to the extent that one component entering the inelastic behavioral range may cause other components to exhibit an inelastic behavior. For example, as inelastic flexural deformations increase, so do shear deformations governed by expanding flexure-shear cracks. Such intricacies in deformation response of concrete members require deformation components to be measured along a member length if they are to be properly understood and modeled.

4.1 Deformation measurements and estimates based on traditional instrumentation

Due to limitations of traditional instrumentation, tests on concrete members often only produced global lateral-load versus lateral-drift relations. Very limited tests with LVDT arrangements along member length, as illustrated in Fig. 2, provided glimpses of the three components of deformations and guided the development of models representing the three deformation components (e.g., Lehman 2004). However, such models were calibrated to the larger body of tests that only provided global force-deformation relations, and exhibit relatively large errors in their estimates (e.g., Priestley 2003, Elwood and Eberhard 2009). The large errors in estimates can be attributed to the lack of distributed deformation data, which has forced the structural engineering community to make many assumptions in model development.

Several models have been proposed that provide an effective stiffness for cracked and un-cracked concrete members (e.g., Sozen 1974; Paulay and Priestley 1992; Priestley 2003; Ghannoum and Moehle 2012b; Elwood and Eberhardt 2009). Member stiffness relations were often derived based on experimental evidence by drawing a secant that intercepts the global force-deformation relation at a desired load level. Typically, the effective stiffness is evaluated at "first yield" (or at first significant inelastic deformations), and is broken down into its components as described in Eq. (1).

$$\Delta_y = \Delta_{FL\text{-}y} + \Delta_{SH\text{-}y} + \Delta_{BS\text{-}y} \tag{1}$$

where Δ_y is the total lateral deformation at "first yield"; $\Delta_{FL\text{-}y}$ is the flexural deformation; $\Delta_{SH\text{-}y}$ is the shear deformation; and $\Delta_{BS\text{-}y}$ is the bar-slip deformation.

To deconstruct global deformation measurements into components, flexural deformations can be evaluated using moment curvature analysis. A moment-curvature relation is computed assuming linear sectional strain profiles. For a given moment distribution along a member length, associated curvatures are evaluated based on the estimated moment-curvature relation, and integrated over the length of a member to obtain rotations and drifts (Fig. 5). For a column with lateral loads applied only at the ends, lateral drift due to flexural deformations can be evaluated using Eq. (2):

$$\Delta_{FL\text{-}y} = \psi_y l^2/6 \tag{2}$$

Based on limited test data (e.g., Lehamn 2004), shear deformations are typically assumed to be small, and are either ignored or estimated using a shear stiffness that is a fraction of the gross shear stiffness (ASCE 41-06).

Bar slip deformations can then be estimated as:

$$\Delta_{BS\text{-}y} = \Delta_y - \Delta_{FL\text{-}y} - \Delta_{SH\text{-}y} \tag{3}$$

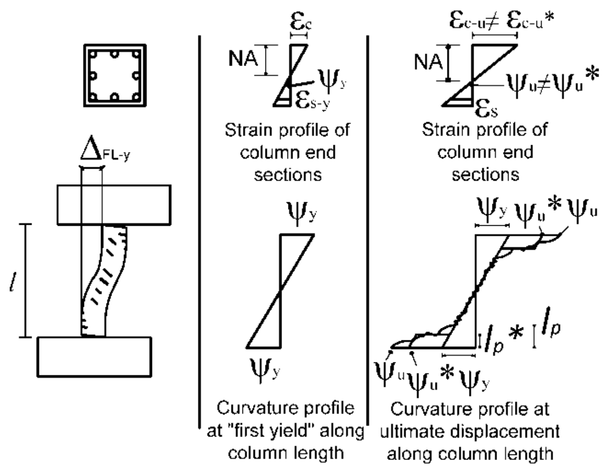

Fig. 5 Flexural deformations

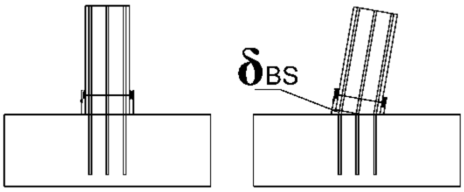

Fig. 6 Traditional measurement of bar-slip

Limited tests have recorded bar-slip induced rotations using the LVDT setup illustrated in Fig. 6 (e.g., Sezen and Moehle 2006). The instrumentation setup is able to provide a reasonable measure of bar-slip induced rotations, but does not allow for direct measurement of the center of rotation about which bar-slip rotations occur, nor the amount bars slip from the foundation. Such measures have always been assumed in bar-slip models (e.g., Ghannoum 2012b).

In the non-linear range of behavior, ductility capacity is a major concern in seismic applications. The ultimate displacement, Δ_u, defines the ductility capacity of a concrete member. The definition of Δ_u depends on the type of failure experienced by a member (i.e., hoop fracture, bar buckling, bar fracture, etc …). Typically, inelastic deformations are estimated through deformations of idealized plastic hinges that are given a length (l_p*) and an ultimate curvature (ψ_u*) at which failure is considered to occur (Fig. 5). Inelastic deformations are added to elastic deformations (Δ_y) by integrating a constant curvature (ψ_u*-ψ_y) over the specified plastic hinge length (l_p*) (Eq. (4)).

$$\Delta_u = \Delta_y + l_p(\psi_u^* - \psi_y)(l - l_p^*) \tag{4}$$

The behavior of a concrete member is however quite different from that described by the idealized plastic hinge models. Inelastic curvatures in concrete members tend to spread over a plastic hinge l_p in a gradual manner up to an ultimate curvature ψ_u (Fig. 5). When simplifying that behavior into a plastic hinge with constant inelastic curvature and comparable area under the curvature diagram to the actual curvature profile, both the plasticity spread and the ultimate curvature experienced by the member (l_p and ψ_u) can be underestimated (ψ_u* and l_p*). Several models have been proposed to estimate plastic hinge length and associated ultimate curvature (e.g., Corley 1966; Priestly *et al*. 1996; Mendis 2001; Bae and Bayrak 2008). Some models specify an ultimate concrete compressive strain from which an ultimate curvature can be calculated based on sectional analysis (e.g., Baker and Amarakone 1965, Corley 1966; Priestly *et al*. 1996). However, traditional instrumentation cannot measure the ultimate concrete compressive strains or the ultimate curvature at failure, nor can they measure accurately the extent of plasticity spread. Thus traditional instrumentation limitations have left many unanswered questions regarding plasticity spread. It is uncertain whether l_p starts spreading at onset of inelastic deformation but stabilizes at a certain deformation or if it continues to spread up to failure. It is also unclear what shape the inelastic curvature profile exhibits and how that shape changes with increasing demands.

4.2 Deformation measurements and estimates based on DIC instrumentation

Many parameters leading to the extraction of lateral drift components and the development of deformation models needed to be assumed or inferred as they could not be measured using traditional instrumentation. The use of DIC technology allows accurate measurement of each component of deformation down to material strains when using high-resolution DIC systems. The UTVS was used to deliver three-dimensional target locations for Experiment 1. The total lateral drift of the column was obtained by averaging the horizontal displacements of the targets on the top beam/footing and subtracting from them the average horizontal displacement of the targets on the bottom beam/footing. While the bottom footing did not slide during the test, the UTVS was able to resolve footing deformations due to applied loads and those were subtracted from all other column movements throughout the test. Deformations tracked by the UTVS were synchronized with data from traditional instruments (i.e., load cells and strain gages).

Curvature profiles along column length were evaluated by calculating the curvature between adjacent horizontal target rows (ψ_i) as the difference in angle of rotation between the two rows divided by distance between them. Flexural deformations were extracted from target displacement values by integrating those curvatures over the height of the column. Fig. 7 illustrates the curvature profiles obtained in Experiment 1 at frame 4206 (corresponding to a column drift ratio of 0.75%) and frame 5510 (corresponding to a column drift ratio of 1.65%). Fig. 7 highlights the large effects of flexural cracking on the curvature profiles of the column. By applying moving-average smoothing to the raw curvature data, more familiar curvature profiles emerge. This figure highlights the ability of the UTVS to track plasticity spread and ultimate curvatures in concrete members. From Fig. 7, it appears that the plastic hinge length remains constant throughout the test, while inelastic curvatures increase as deformation demands increase.

The slip of longitudinal bars from adjacent members causes rigid body rotation of a column about the interface between the column and adjacent members (Fig. 8). Various assumptions have been made about the amount longitudinal bars slip from adjacent members (δ_{bs} in Fig. 8) and the

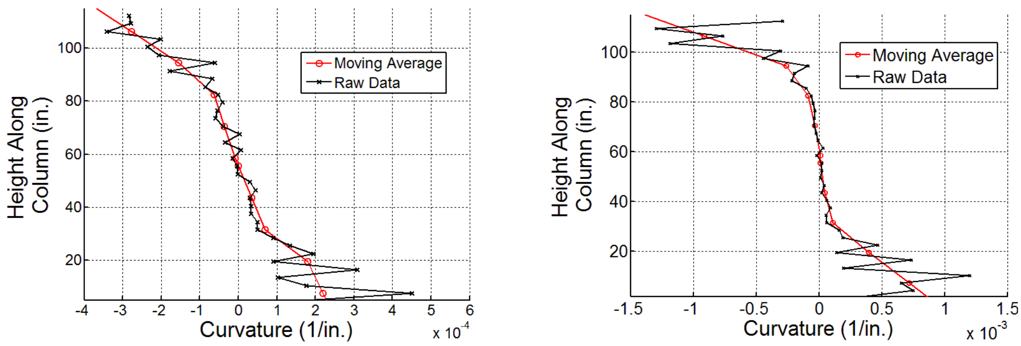

Fig. 7 Measured curvatures at frames 4206 = 0.75% drift ratio, and 5510 = 1.65% drift ratio – Experiment 1 (1 in. = 25.4 mm)

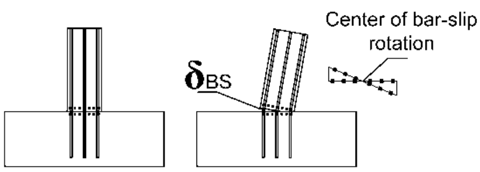

Fig. 8 UTVS measurement of bar-slip

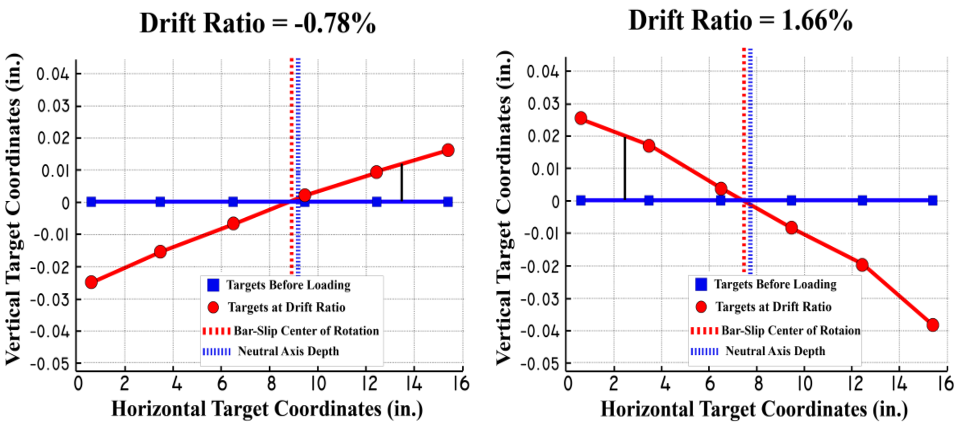

Fig. 9 Bar-slip induced rotations – Experiment 1 (1 in. = 25.4 mm)

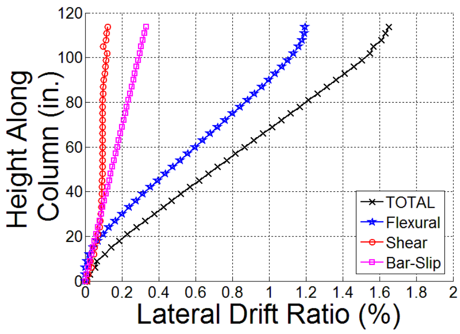

Fig. 10 UTVS measured displacement components at frame 5510 (1 in. = 25.4 mm)

center of rotation of bar-slip induced rotations. δ_{bs} is typically estimated in bar-slip models by assuming a simple bond stress model that is calibrated to global column deformations (e.g., Lehman 2004; Saatcioglu and Ozcebe 1989). Postulated centers of rotation include the edge ofthe column and the flexural neutral axis. DIC systems allow the direct measurement of relative rotations between the outermost column target rows and target rows on footings (Fig. 9). As can be seen in Fig. 9, DIC data provide accurate measures of the amount longitudinal bars are slipping from the adjacent footings, δ_{bs}. Furthermore, the DIC data clearly show the center of rotation of the outermost column target rows. In Fig. 9, the estimated location of the flexural neutral axis, based on sectional analysis, is plotted. As can be seen in the figure, the center of rotation of the bar-slip induced rotation matches well with the estimated location of the neutral axis. The DIC data recorded in Experiment 1 therefore corroborates a key assumption in bar-slip models for the column tested; something that could not be done prior to DIC data.

Column shear deformations (Δ_{SH}) can be extracted from DIC data by subtracting the lateral drift due to flexure and bar-slip from the total column lateral drift. Shear deformations along the length of the column can be evaluated between successive rows of targets as well. The end result of deconstructing column deformations in to the three main components is illustrated in Fig. 10

and Fig. 11. One can see in Fig. 10 the interactions between shear and flexural deformations. As the ratio of moment to shear forces increases along the length of the column, shear deformations are observed to increase more markedly indicating a softening of the shear response with larger applied moments. Conversely, the plastic hinge length observed in Fig. 7 seems to correlate with regions of higher shear deformations indicating that the tension shift phenomenon (Paulay and Priestley 1975) may be more influential than previously thought in plasticity spread. The ability to measure variations of shear and flexural deformations along the length of a member provides a wealth of interaction data that can be used to develop deformation-interaction diagrams akin to strength interaction diagrams the structural engineering field is familiar with. Figs. 10 and 11 also show the magnitude of the various deformation components and how these proportions vary with increasing force and deformation demands. The cyclic

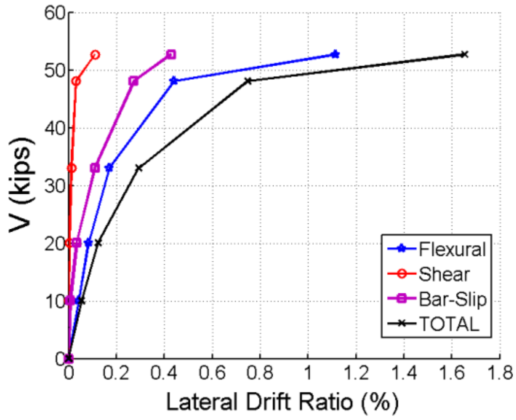

Fig. 11 Measured backbone displacement components – Experiment 1 (1 kip = 4.45 kN)

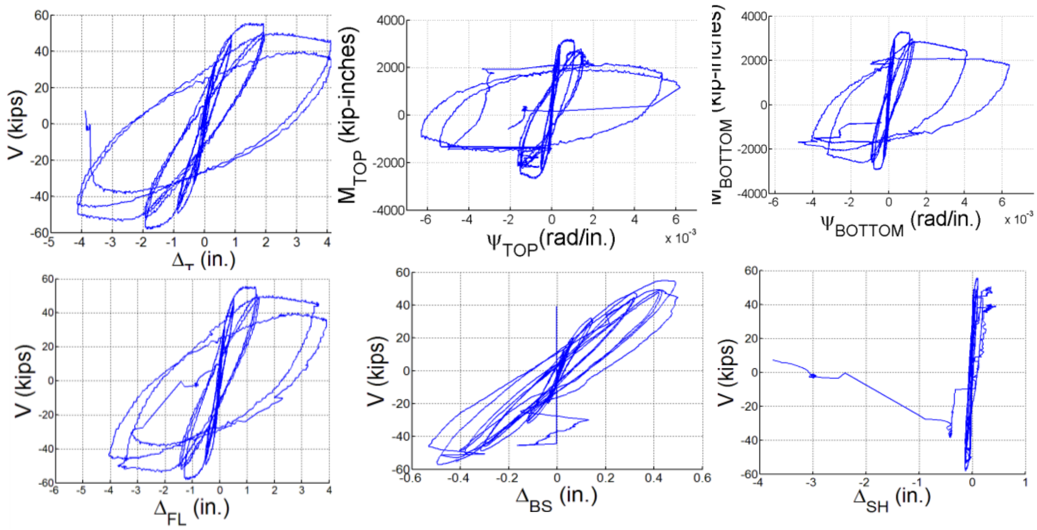

Fig. 12 UTVS cyclic deformation measurements – Experiment 1 (1 in. = 25.4 mm, 1 kip = 4.45 kN)

response of all deformation components and the cyclic moment-curvature responses at the top and bottom of the column are plotted in Fig. 12. DIC data were used to produce the plots in Fig. 12 that highlight the capabilities of such a powerful measurement tool.

In summary, DIC data can be very useful in deconstructing and understanding the complex interactions that govern the deformation behavior of concrete members. DIC data can be used to improve the fidelity of our behavioral models and lead to analytical simulation tools with higher accuracy. As novel systems are explored (e.g., Macchi *et al*. 1996) or the seismic performance of older non-conventional members need to be assessed (e.g., Verderame *et al*. 2008), the comprehensive nature of DIC data can result in the development of improved understanding and simulation capabilities with fewer tests than would be needed if the limited data of traditional instrumentation is only available. DIC data can also be very useful when investigating material interactions in retrofit techniques using external applications of Fiber-Reinforced Polymers (FRP) (e.g., Kim *et al*. 2011).

5. DIC material strain measurements

Given sufficiently high resolution, such as that achieved by the UTVS, measurements of three-dimensional movements of known locations (i.e., targets) on a test specimen can be used to calculate surface material-strains. The UTVS can resolve surface strains to within 10^{-4} for a field of view of about 8ft (2.44 m); a strain resolution that is on the order of the cracking strain of concrete. Furthermore, DIC data can be used to infer internal material strains from surface strain measurements, as will be demonstrated. With a complete material-strain record, improved behavioral understanding can be achieved as the flow of forces can be observed through compression-strain fields and crack patterns. Previously unseen mechanisms and interactions between materials and forces can be uncovered and implemented in strain-based analytical models such as fiber-section or continuum finite-element models; thereby improving their fidelity in capturing failure mechanisms. Direct calibrations of strain-based models at the strain level will further improve their accuracy.

After completing a tracking, calibration, and triangulation process, the UTVS provided the three-dimensional movement of each target for the duration of Experiment 2. The surface targets arranged in a rectangular mesh were used as nodal points for bilinear-strain quadrilateral elements. Assuming that strains varied linearly between targets, the measured x-directional (horizontal, ε_x), y-directional (vertical, ε_y), shear, and principal strains were determined (ε_1 = largest principal strain and ε_2 = smallest principal strain). The center of the quadrilateral elements and their corresponding strains are plotted as contours in Fig. 13. The photograph and strain contour plots in Fig. 13 correspond to one instance in time during the experiment at frame number 11,392, which corresponds to the first excursion to a lateral drift ratio of +3.0%. In Fig. 13 and subsequent figures, a positive drift ratio indicates column movement to the right. Blank areas in the contour plots indicate that the ability to track targets was lost or that strains at that location exceeded a prescribed strain limit. In Fig 13, the blank areas correspond to element strains exceeding the prescribed strain limits of ±0.1.

Fig. 13 illustrates the surface strain measurement capabilities of the UTVS. In the plot of the principal strain ε_2, one can clearly see the magnitude of compressive strains in compression struts. In the bottom half of the figure, a compression strut can be seen fanning from the bottom right corner of the column out to mid height of the column, with decreasing compressive strains as the width of the strut increases. Contour plots in Fig 13 also show areas of concrete spalling and large tensile strains indicative of large cracks. Areas of high horizontal strains (ε_x) are indicative of large core dilatations and confinement demands on hoops.

DIC measurements of surface strains can be used to estimate internal material strains. To illustrate this point, the strains between a strain gauge attached to the outer surface of a hoop and the strain in the *x*-direction of the closest surface element were compared. The selected strain gauge and surface element were located 25 in. (635 mm) from the bottom of the column and in the path of an inclined crack. In Fig. 14, strains recorded by the hoop strain-gauge and surface-element strains are compared. As the width of the inclined crack increased, the hoop and element peak tensile strains converged. However, as the lateral drift reversed, the hoop lost more than half of its

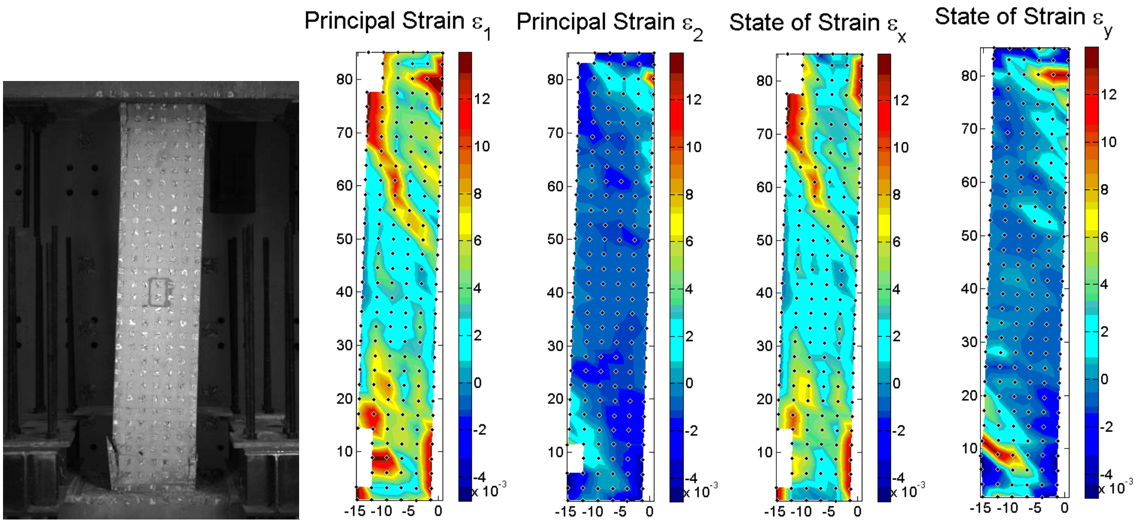

Fig. 13 Column surface strains at frame number 11,392 (first drift excursion to +3.0%); positive strain values correspond to tensile strains – Experiment 2

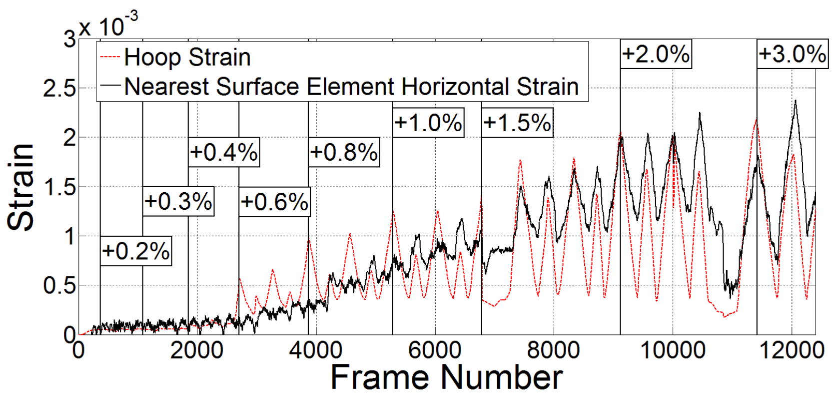

Fig. 14 Comparison between hoop strain and strain of the nearest surface element

peak tensile strains while the surface element lost only a small fraction of its peak strain. Thus, surface cracks remained open when the lateral load was being reversed, which indicates that much of the load transferred across the crack was transferred through the steel. Such observations of lag between steel strains and concrete crack-width have been reported in some studies such as those conducted on the reverse cyclic behavior of shear panels (e.g., Gérin and Adebar 2009). In such studies, manual crack width measurements could only be conducted at limited locations and at certain load levels. DIC systems can continuously monitor surface tensile strains that can be used to estimate crack widths and internal steel strains. Fig. 14 confirms that internal material strains can be inferred reliably from surface strains measurements; something that cannot be done using data from visual crack measurements.

Figs. 13 and 14 thus demonstrate that high-resolution DIC systems can provide external as well as internal material strain distributions, from which associated material stress distributions can be estimated. Such measurements usher a new era in behavioral inference and analytical-model formulation and calibration from structural testing.

6. Damage evaluations

Damage in reinforced concrete members is typically judged based on crack widths, areas of spalled concrete, and in cases of extreme damage, on steel-bar damage and permanent deformations. Much subjectivity is introduced in the measurement of the above quantities during structural testing and post-event damage assessments. Crack widths are typically measured by hand and are subject to user error and interpretation. Furthermore, cracks are typically measured at limited locations giving only a glimpse of the extent of cracking. Areas of spalled concrete are often visually determined and plots shading the spalled areas produced. High-resolution DIC systems offer a means of evaluating damage in concrete members in an objective and comprehensive fashion. Moreover, DIC systems are able to track damage progression throughout structural tests, and if used in the field, throughout a seismic event.

Using DIC surface-strain data, crack widths can be estimated over the entire specimen surface, from which crack-width based damage indices can be evaluated. To illustrate these capabilities, the average and maximum crack widths (w_c) evaluated at each recorded image frame in Experiment 2 are plotted in Fig. 15. For a given frame, a crack was assumed to have formed within a quadrilateral surface-element when the element's maximum principal tensile strain (ε_1) exceeded an assumed cracking strain, $\varepsilon_{cr}=f'_t/E_c=7.5/57000 = 1.3 \times 10^{-4}$ (with f'_t = concrete ultimate tensile strain, E_c = concrete modulus of elasticity, values are based on provisions of ACI 318-11). After an initial crack formed in an element, the average elastic strain in adjacent uncracked concrete was assumed to be half the cracking strain. Thus, the crack width within surface elements can be calculated by subtracting half of the cracking strain from the maximum principal tensile strain and then multiplying the modified strain by the surface elements' length perpendicular to the crack (Eq. (5)). Since the surface elements are square, their lengths perpendicular to an inclined crack vary with crack inclination. An equivalent length ($L_{equiv.}$) was used for all crack inclinations to simplify the crack width evaluation procedure. The equivalent length was taken as the diameter of a circle of equivalent area to the square elements.

$$w_c=\left(\varepsilon_1-{}^{\varepsilon_{cr}}/_{2}\right)*L_{equiv.} \tag{5}$$

As can be seen in Fig. 15, crack-width growth remained low up to a drift ratio of 1.5%, with each crack being able to close nearly as much as it had opened with each drift reversal. However, at a drift ratio of 1.5%, the maximum crack widths began to grow rapidly. When the lateral load was removed during the load reversal, the cracks were unable to close resulting in a maximum crack width plateau as seen around frame number 8,000. Moreover, the large variations between the average and maximum crack widths indicate that large localized cracks began to form rather than moderately sized well-distributed cracks. It is interesting to note that large increases in maximum crack-width are seen in the first loading cycle to a drift ratio of -2.0%, just after a +2.0% drift-ratio excursion; as opposed to occurring during the first excursion to that drift level. Maximum crack widths subsequently stabilized as drift excursions reached a drift ratio of + 3.0%. The data clearly show a threshold deformation at which this particular column sees large increases in maximum crack widths. Such threshold demands at which large damage is observed are difficult to pinpoint using traditional damage measurement techniques.

Since the crack widths are evaluated for all elements and all frames, a crack-width intensity measure can be constructed to help quantify overall crack-induced damage. The crack-width intensity measure is defined as the summation of element crack widths divided by the total element surface area. As indicated by Fig 16, the crack-width intensity rose steadily through a drift ratio of 2.0%. Note that from frame number 10,451 to 11078, the column was axially unloaded at the end of the first day of testing and reloaded on the second day of testing.

DIC data can also measure the area of crushed or spalled concrete throughout a test. A threshold compressive strain of -4×10^{-3} was used to identify areas with crushed concrete. A surface element was considered damaged if its minimum principal strain, ε_2, ever exceeded the

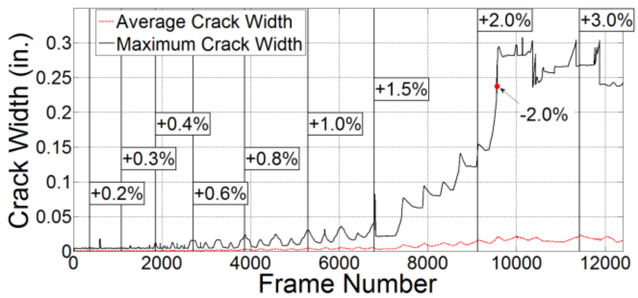

Fig.15 Average and maximum column crack widths (1 in. = 25.4 mm)

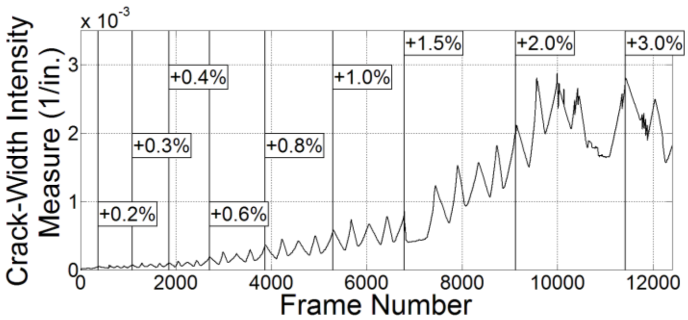

Fig.16 Cracking damage (1in. = 25.4 mm)

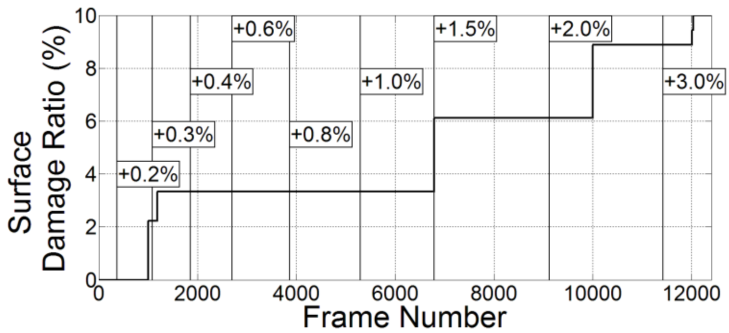

Fig.17 Crushing damage

assumed crushing strain. The surface damage ratio was determined by dividing the summation of the surface area of all the damaged elements by the total element surface area. Measurable crushing damage was found to have occurred at drift ratios of 0.3%, 1.5%, 2.0%, and 3.0% (Fig. 17).

Here again it is interesting to note that at around frame number 10,000, significant crushing-damage was observed while cycling for the second time to a drift ratio of +2.0%. This crushing damage correlates with the sharp increase in maximum crack widths observed in Fig. 15.

7. Conclusions

The capabilities of a high-resolution DIC system dubbed the UTVS were presented within the context of deformation measurements of full-scale concrete columns tested under reversed cyclic loading. The UTVS was developed to have very high-resolution such that material strains on the order of the cracking stain of concrete could be measured on the surface of full-scale structural members. The three-dimensional surface deformations recorded by the UTVS were shown to produce quantities that had never been recorded to such high resolution and definition. The DIC system was able to resolve the full profiles of column curvatures, rotations, plasticity spread, shear deformations, and bar-slip induced rotations. Measurements of the amount of slip of longitudinal bars from adjacent members were demonstrated, as well as those of the center of the bar-slip induced rotations; quantities that could not be measured prior to the use of DIC. Material strains at the surface of structural members were shown to correlate well with internal material strains.

High-resolution DIC data can be used to provide objective measures of damage accumulation that are directly related to cracking and spalling damage. Such measures are crucial within the performance-based design and assessment methodology, when limiting damage is desired for immediate-occupancy or limited-damage performance objectives. DIC damage measures contrast prevailing proxy damage indices based on member force-deformation data, and subjective damage measures obtained using visual inspection. As more DIC test data becomes available, damage models can be developed and fragility curves produced to inform designers about engineering demand parameters that generate damage in excess of target damage objectives.

Data derived from high-resolution DIC systems is shown to be of great use in advancing the state of behavioral knowledge, calibrating behavioral and analytical models, and improving simulation accuracy.

Acknowledgments

The research described in Experiment 2 was partially supported by NUCOR Steel Seattle and the Concrete Reinforcing Steel Institute. The high-resolution DIC system (UTVS) was developed at the Ferguson Structural Laboratory of the University of Texas at Austin with the help of Eric Schell and Matthew Homer.

References

American Concrete Institute (ACI) Committee 318 (2011), "Building code requirement for structural concrete (ACI 318-11) and commentary", Farmington Hills, MI: American Concrete Institute

American Society of Civil Engineers/Structural Engineering Institute (ASCE/SEI) Committee 41 (2007), "Seismic Rehabilitation of Existing Structures", *ASCE 41-06* Reston, VI, 428.

ASTM Standard A706/A706M-13 (2013), "Standard specification for low-alloy steel deformed and plain bars for concrete reinforcement", ASTM International, West Conshohocken, PA

ASTM Standard A615/A615M-13 (2013), "Standard specification for deformed and plain carbon-steel bars for concrete reinforcement", ASTM International, West Conshohocken, PA

Bae, B. and Bayrak, O. (2008), "Plastic hinge length of reinforced concrete columns", *ACI Struct. J.*, **105**(3), 290-300

Baker, A. and Amarakone, A. (1965), "Inelastic hyperstatic frames analysis", *ACI Special Publication*, **12**, 85-142

Corley, W.G. (1966), "Rotational capacity of reinforced concrete beams", *Proceedings of the American Society of Civil Engineers*, **ST 5**, 121-146

Cosenza E., Manfredi, G. and Ramasco, R. (1993), "The use of damage functionals in earthquake engineering: a comparison between different models", *Earthq. Eng. Struct. Dyn.*, **22**, 855-868

Eleftheriadou, A.K. and Karabinis, A.I. (1999), "Seismic vulnerability assessment of buildings based on damage data after a near field earthquake", *Earthq. Struct.*, **3**(2), 117-140

Elwood, K.J. and Eberhard, M.O. (2009), "Effective stiffness of reinforced concrete columns", *ACI Struct. J.*, **106**(4), 476-484

Federal Emergency Management Agency (FEMA) (1997), "NEHRP Guidelines for the Seismic Rehabilitation of Buildings", FEMA-273, Federal Emergency Management Agency, Washington, DC, 435.

Federal Emergency Management Agency (FEMA) (2007), *Interim Testing Protocols for Determining the Seismic Performance Characteristics of Structural and Nonstructural Components*, FEMA-461, Federal Emergency Management Agency, Washington, DC, 138.

Ghannoum, W.M., and Moehle, J.P. (2012a), "Shake-table tests of a concrete frame sustaining column axial failures", *ACI Struct. J.*, **109**(3), 393-402.

Ghannoum, W.M and Moehle, J.P. (2012b), "Dynamic collapse analysis of a concrete frame sustaining column axial failures", *ACI Struct. J.*, **109**(3), 403-412.

Sezen, H. and Moehle, J.P. (2006), "Seismic tests of concrete columns with light transverse reinforcement", *ACI Struct. J.*, **103**(6), 842-849

Ghannoum, W.M., Saouma, V., Haussmann, G., Polkinghorne, K., Eck, M. and Kang, D.H. (2012), "Experimental investigations of loading rate effects in reinforced concrete columns", *J. Struct. Eng.*, **138**(8), 1032-1041

Gérin, M. and Adebar, P. (2009), "Simple rational model for reinforced concrete subjected to seismic shear", *J. Struct. Eng.*, **135**(7), 753-761).

IAAE 1996 - IAEE (1996), Regulations for Seismic Design. International Association for Earthquake

Engineering, a world list.

Kim, Y., Quinn, K.T., Satrom, C.N., Ghannoum, W.M. and Jirsa, J.O. (2011), "Shear strengthening RC T-beams using CFRP laminates and anchors", *ACI Special Publication*, SP**275**-36, 1-18.

Leborgne, M.R., (2012), "Modeling the post shear failure behavior of Reinforced concrete columns", Ph.D. dissertation, The University of Texas at Austin, Austin, TX.

Lehman, D., Moehle, J., Mahin, S., Calderone, A. and Henry, L. (2004), "Experimental evaluation of the seismic performance of reinforced concrete bridge columns", *J. Struct. Eng.*, **130**(6), 869-879.

Lynn, A.K. (2001), "Seismic evaluation of existing reinforced concrete building columns", Ph.D. dissertation, University of California at Berkeley, Berkeley, CA.

Mathworks (2014), "Matlab Image Processing Toolbox", http://www.mathworks.com/products/image/

Macchi, G., Pinto, P.E. and Sanpaolesi, L. (1996), "Ductility requirements for reinforcement under Eurocodes", *Struct. Eng. Int.*, **6**(4), 249-254.

Mendis, P. (2001), "Plastic hinge lengths of normal and high-strength concrete in flexure", *Adv. Struct. Eng.*, **4**(4), 189-195.

National Instruments, 2014, "NI Vision Development Toolbox", http://www.ni.com/labview/vision/

Park, Y.J and Ang, A.H.S. (1985), "Mechanical seismic damage model for reinforced concrete", *ASCE*, **111**(4), 722-757

Paulay, T. and Priestley, M.J.N. (1992), *Seismic Design of Reinforced Concrete and Masonry Buildings*, John Wiley and Sons, Canada

Priestley, M.J.N., Seible, F. and Calvi, G.M. (1996), *Seismic Design and Retrofit of Bridges*, John Wiley and Sons, Inc., New York

Priestley, M.J.N. (2003), "Myths and fallacies in earthquake engineering, revisited" (In the Ninth Mallet Milne Lecture), Rose School, Pavia, Italy., 9-31

Saatcioglu M. and Ozcebe, G. (1989), "Response of reinforced concrete columns to simulated seismic loading", *ACI Struct. J.*, **86**(1), 3-12

Verderame, G.M., Fabbrocino, G. and Manfredi, G. (2008), "Seismic response of RC columns with smooth reinforcement. Part II: Cyclic tests", *Eng. Struct.*, **30**(9), 2289-2300